J|A|C|S ARTICLES

Published on Web 07/02/2009

Control and Characterization of Cyclopentene Unimolecular Dissociation on Si(100) with Scanning Tunneling Microscopy

Nathan L. Yoder, James S. Fakonas, and Mark C. Hersam*

Department of Materials Science and Engineering, Department of Chemistry, Northwestern University, 2220 Campus Drive, Evanston, Illinois 60208-3108

Received February 10, 2009; E-mail: m-hersam@northwestern.edu

Abstract: Dissociation of individual cyclopentene molecules on the Si(100) surface is induced and investigated using cryogenic ultrahigh vacuum scanning tunneling microscopy (STM). Using a secondary feedback loop during elevated tunneling current and sample biasing conditions, the cyclopentene dissociation products are isolated and then characterized with atomic-scale spatial resolution. Using multibias STM and density functional theory, the cyclopentene dissociation products are shown to consist of a C_5H_7 fragment and an individual H atom. The C_5H_7 fragment contains a C=C double bond and is bound to the Si(100) surface via a single Si−C covalent bond, while the individual H atom can be induced to hop between two sites on a single silicon dimer with the STM tip. This study shows that the use of feedback control during STM-induced single molecule reactions allows transient reaction products to be captured and thus more thoroughly studied. While demonstrated here for cyclopentene on Si(100), this feedback-controlled approach can likely be applied to a wide array of chemical reactions on semiconductor surfaces.

Introduction

Fundamentally, chemical reactions can be described in terms of interactions between individual molecules, surfaces, and energy. The scanning tunneling microscope (STM)[1−3] has enabled insight and control at this fundamental level due to its atomic-scale spatial resolution imaging and manipulation capabilities. In recent years, the STM has been employed to induce and characterize a variety of single molecule phenomena including reversible vertical switching,[4,5] lateral displacement,[6−8] rotation,[9−12] dissociation,[13−16] desorption,[17−22] and adsorption configuration changes.[23] These experimental studies have been coupled with theoretical calculations to further the understanding of both reversible and irreversible chemistry on surfaces.[24−28]

From a technological perspective, there has been increasing interest in combining the properties of organic molecules with the established capabilities of semiconductor surfaces.[29,30] This interface is especially relevant for the fields of molecular electronics[31−35] and chemical and biological sensing,[36,37] which

(1) Binnig, G.; Rohrer, H.; Gerber, C.; Weibel, E. *Phys. Rev. Lett.* **1982**, *49*, 57–61.
(2) Ho, W. *J. Chem. Phys.* **2002**, *117*, 11033–11061.
(3) Hla, S. W.; Rieder, K. H. *Annu. Rev. Phys. Chem.* **2003**, *54*, 307–330.
(4) Eigler, D. M.; Lutz, C. P.; Rudge, W. E. *Nature* **1991**, *352*, 600–603.
(5) Stipe, B. C.; Rezaei, M. A.; Ho, W. *Phys. Rev. Lett.* **1997**, *79*, 4397–4400.
(6) Eigler, D. M.; Schweizer, E. K. *Nature* **1990**, *344*, 524–526.
(7) Bartels, L.; Meyer, G.; Rieder, K. H. *Phys. Rev. Lett.* **1997**, *79*, 697–700.
(8) Basu, R.; Tovar, J. D.; Hersam, M. C. *J. Vac. Sci. Technol. B* **2005**, *23*, 1785–1789.
(9) Stipe, B. C.; Rezaei, M. A.; Ho, W. *Science* **1998**, *279*, 1907–1909.
(10) Stipe, B. C.; Rezaei, M. A.; Ho, W. *Phys. Rev. Lett.* **1998**, *81*, 1263–1266.
(11) Lastapis, M.; Martin, M.; Riedel, D.; Hellner, L.; Comtet, G.; Dujardin, G. *Science* **2005**, *308*, 1000–1003.
(12) Wang, B.; Zheng, X. L.; Michl, J.; Foley, E. T.; Hersam, M. C.; Bilic, A.; Crossley, M. J.; Reimers, J. R.; Hush, N. S. *Nanotechnology* **2004**, *15*, 324–332.
(13) Dujardin, G.; Walkup, R. E.; Avouris, P. *Science* **1992**, *255*, 1232–1235.
(14) Martel, R.; Avouris, P.; Lyo, I. W. *Science* **1996**, *272*, 385–388.
(15) Stipe, B. C.; Rezaei, M. A.; Ho, W.; Gao, S.; Persson, M.; Lundqvist, B. I. *Phys. Rev. Lett.* **1997**, *78*, 4410–4413.
(16) Sloan, P. A.; Palmer, R. E. *Nature* **2005**, *434*, 367–371.
(17) Shen, T. C.; Wang, C.; Abeln, G. C.; Tucker, J. R.; Lyding, J. W.; Avouris, P.; Walkup, R. E. *Science* **1995**, *268*, 1590–1592.
(18) Stokbro, K.; Thirstrup, C.; Sakurai, M.; Quaade, U.; Hu, B. Y. K.; Perez-Murano, F.; Grey, F. *Phys. Rev. Lett.* **1998**, *80*, 2618–2621.
(19) Hersam, M. C.; Guisinger, N. P.; Lyding, J. W. *Nanotechnology* **2000**, *11*, 70–76.
(20) Yoder, N. L.; Guisinger, N. P.; Hersam, M. C.; Jorn, R.; Kaun, C. C.; Seideman, T. *Phys. Rev. Lett.* **2006**, *97*, 187601.
(21) Alavi, S.; Rousseau, R.; Patitsas, S. N.; Lopinski, G. P.; Wolkow, R. A.; Seideman, T. *Phys. Rev. Lett.* **2000**, *85*, 5372–5375.
(22) Walsh, M. A.; Hersam, M. C. *Annu. Rev. Phys. Chem.* **2009**, *60*, 193–216.
(23) Riedel, D.; Bocquet, M.-L.; Lesnard, H.; Lastapis, M.; Lorente, N.; Sonnet, P.; Dujardin, G. *J. Am. Chem. Soc.* **2009**, *131*, 7344–7352.
(24) Salam, G. P.; Persson, M.; Palmer, R. E. *Phys. Rev. B* **1994**, *49*, 10655–10662.
(25) Gao, S. W.; Persson, M.; Lundqvist, B. I. *Phys. Rev. B* **1997**, *55*, 4825–4836.
(26) Seideman, T. *J. Chem. Phys.* **1997**, *106*, 417–431.
(27) Seideman, T.; Guo, H. *J. Chem. Phys.* **1997**, *107*, 8627–8636.
(28) Boendgen, G.; Saalfrank, P. *J. Phys. Chem. B* **1998**, *102*, 8029–8035.
(29) Guisinger, N. P.; Greene, M. E.; Basu, R.; Baluch, A. S.; Hersam, M. C. *Nano Lett.* **2004**, *4*, 55–59.
(30) Guisinger, N. P.; Yoder, N. L.; Hersam, M. C. *Proc. Natl. Acad. Sci. U.S.A.* **2005**, *102*, 8838–8843.
(31) Aviram, A.; Ratner, M. A. *Chem. Phys. Lett.* **1974**, *29*, 277–283.
(32) Tour, J. M. *Acc. Chem. Res.* **2000**, *33*, 791–804.
(33) Lindsay, S. M.; Ratner, M. A. *Adv. Mater.* **2007**, *19*, 23–31.
(34) Hersam, M. C.; Reifenberger, R. G. *MRS Bull.* **2004**, *29*, 385–390.
(35) Tao, N. J. *Nat. Nanotechnol.* **2006**, *1*, 173–181.
(36) Lin, Z.; Strother, T.; Cai, W.; Cao, X. P.; Smith, L. M.; Hamers, R. J. *Langmuir* **2002**, *18*, 788–796.
(37) Cui, Y.; Wei, Q. Q.; Park, H. K.; Lieber, C. M. *Science* **2001**, *293*, 1289–1292.

can benefit substantially from interfacing with established semiconductor electronics. A key challenge in this area is to understand how single molecules respond to electric fields and currents, which is vital to engineering successful devices. Additionally, this knowledge is of critical importance to understanding and constructing molecular-scale mechanical systems.[38,39]

The above studies demonstrate the suitability of the STM to address these questions. Previous work in this area has focused on characterizing the desorption of cyclopentene from p-Si(100) at low temperature,[20] which was determined to be a resonance-mediated single electron process. The desorption yield as a function of sample bias and tunneling current was determined by desorbing a large number of molecules with a blanket dose of electrons. This method is an efficient strategy for gathering statistical information about the desorption phenomenon but does not allow for more detailed studies of reaction intermediates, since it is difficult to avoid overdosing the reaction products with excess electrons. In many cases, overdosing can present a problem since the reaction products might also be susceptible to electric currents or fields.

A method for controlling the exposure of potentially sensitive surface species was reported in the context of high resolution lithography on H−Si(100), known as feedback-controlled lithography (FCL).[19] This technique employs a second feedback loop to detect changes in either the tunneling current or the tip−sample separations that are indicative of a change in the local density of states due to the desorption of a hydrogen atom. This same technique can be applied to the study of single molecule chemical reactions at the nanometer length scale using the STM. In fact, a similar technique was applied to the controlled dehydrogenation of acetylene on Cu(100).[40] These methods of feedback-controlled chemistry (FCC) offer an additional level of control over such reactions by preventing subsequent electron- or electric field-induced processes that might result from additional exposure of reaction products to tunneling electrons. For more detailed information regarding the specifics of the feedback-controlled manipulation method, the reader is referred to the original FCL paper by Hersam and co-workers.[19] A key criterion for the success of these techniques is that the lifetime of the reaction product or intermediate is longer than the time necessary to detect the conformational change and terminate the flow of electrons. In this paper, we apply the FCC technique to isolated organic molecules on a semiconductor surface, thus allowing for the study of cyclopentene dissociation on Si(100).

Experimental Methods

All experimental measurements were performed on a home-built cryogenic variable-temperature ultrahigh vacuum (UHV) STM operating at a pressure of $\sim 2 \times 10^{-11}$ Torr.[41] Unless stated otherwise, the experiments were performed at the base temperature of 8 K. STM tips were prepared from Pt/Ir wire (90% Pt, 10% Ir) and electrochemically etched in a concentrated $CaCl_2$ solution. The samples were prepared from wafers of highly n-type (arsenic doped) Si(100), which were purchased from Virginia Semiconductor with a resistivity of <0.005 Ω-cm. The wafers were cut to size (6 mm × 10 mm) and cleaned by ultrasonication in 2-propanol for 5 min before introduction into the vacuum system via a load-lock. Prior to the experiment, the samples were degassed in vacuum for 12 h at 600 °C and subsequently flashed repeatedly at 1250 °C for 30 s. Next, the bare Si(100) surface was imaged at room temperature to confirm the cleanliness of the sample. Typical imaging conditions are in the range of ±2−3 V for the sample bias and 0.1−1 nA for the tunneling current.

The cyclopentene molecules were purchased from Sigma-Aldrich and loaded into a glass vial that is interfaced to the UHV-STM chamber via a precision leak valve. The vial was sonicated in acetone and isopropanol as an initial cleaning step. It was subsequently mounted to the STM chamber and simultaneously heated with an acetylene torch and pumped on with a turbomolecular pump. The vial was then sealed and brought into a controlled atmosphere glovebox (nitrogen atmosphere, 1−2 ppm of H_2O and O_2). The cyclopentene was transferred directly to the clean vial in the glovebox to minimize oxygen and water contamination. Finally, the full vial was attached to the chamber and subjected to 20 freeze−pump−thaw cycles to remove dissolved gases from the liquid. To dose the sample for single-molecule experiments, the cyclopentene molecules were introduced into the vacuum chamber via a precision leak valve to a pressure of 1×10^{-9} Torr for ∼100 s, giving a total dose of 0.1 Langmuir. The sample was then imaged at room temperature to confirm that the desired coverage of molecules was achieved, at which point the microscope was cooled to 8 K for cryogenic temperature experiments.

During an FCC experiment, the surface is initially scanned at benign imaging conditions (typically −2.0 V, 0.1−0.2 nA). The primary feedback loop remains on, and the STM tip is positioned directly above an adsorbate of interest. The current and voltage are then adjusted to the desired conditions (typically more perturbative), and the second feedback loop is engaged to monitor changes in the tunneling current or the tip height. Threshold values are specified for these parameters, expressed in Å (ΔZ) or as a percentage of the total current (ΔI). To minimize the effects of noise, a minimum threshold time (Δt) is also specified. When ΔI is used to trigger the second feedback loop, Δt is typically ∼100 μs to detect the event before the primary feedback loop adjusts the tip height and reestablishes the tunneling current. When ΔZ is used as the trigger, this restriction is no longer necessary and the threshold time can be arbitrarily long. However, in an effort to minimize perturbation to reaction products or neighboring adsorbates, Δt values of 100 μs to 100 ms are typically used.

Computational Methods

A $Si_{21}H_{20}$ cluster was chosen for this study to simulate the local environment of the adsorbates. The cluster was constructed in HyperChem Release 7 (Hypercube, Inc., Gainesville, FL) and optimized initially with molecular mechanics. These geometries were further refined using the Q-CHEM 2.1 quantum chemistry software.[42] All calculations in Q-CHEM were performed within density functional theory utilizing the B3LYP[43] hybrid exchange-correlation functional. Following molecular mechanics, the structures were optimized at an intermediate level with a 3-21G Pople-style all-electron basis set of Gaussian functions. The final optimization was performed with a 6-31G* all-electron basis set for all atoms. The simulated STM images were generated by first calculating the values of the one-electron wave functions in Q-CHEM on a grid of points separated by 0.133 Å. Next, these values were imported into Matlab (The MathWorks, Natick, MA), and squared to give the state densities for alpha and beta electrons. To identify which orbitals to include, we assumed that the Fermi level of the substrate was at the center of the HOMO−LUMO gap of the cluster, and included all filled orbitals whose energies fell within the experimental bias window (0 to −2 V). The state

(38) Seideman, T. *J. Phys.: Condens. Matter* **2003**, *15*, R521−R549.
(39) Comtet, G.; Dujardin, G.; Mayne, A. J.; Riedel, D. *J. Phys.: Condens. Matter* **2006**, *18*, S1927−S1934.
(40) Lauhon, L. J.; Ho, W. *Phys. Rev. Lett.* **2000**, *84*, 1527–1530.
(41) Foley, E. T.; Yoder, N. L.; Guisinger, N. P.; Hersam, M. C. *Rev. Sci. Instrum.* **2004**, *75*, 5280–5287.
(42) Kong, J. *J. Comput. Chem.* **2000**, *21*, 1532–1548.
(43) Becke, A. D. *J. Chem. Phys.* **1993**, *98*, 5648–5652.

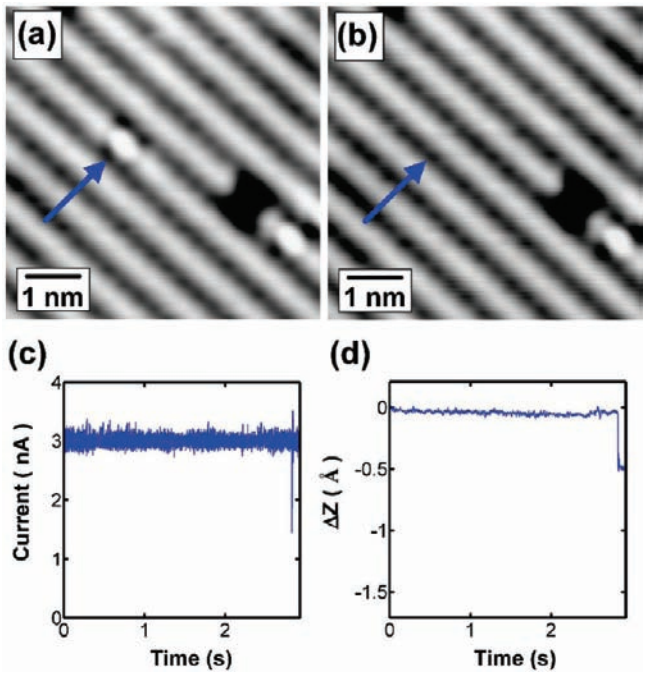

Figure 1. Constant-current STM images (−2 V, 0.1 nA) (a) before and (b) after desorption of an individual cyclopentene molecule (blue arrow) from the Si(100) surface. Plots of (c) tunneling current and (d) change in tip height during FCC show an instantaneous drop in current upon cyclopentene desorption, followed by motion of the tip toward the surface.

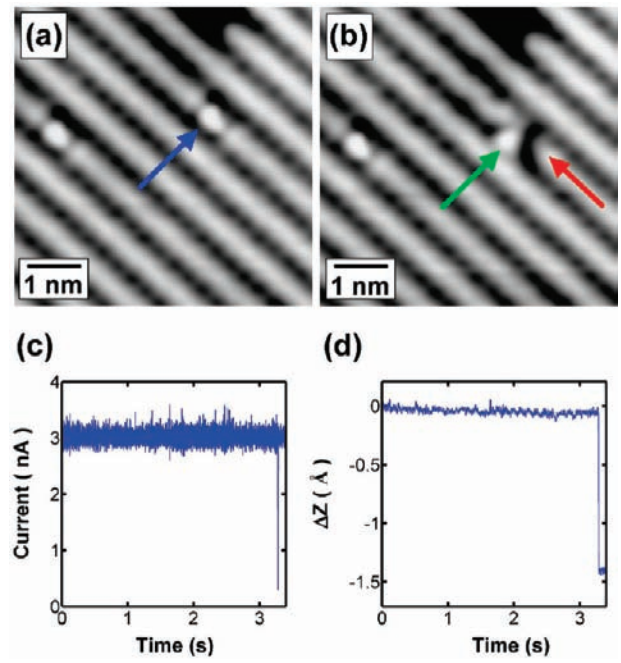

Figure 2. Constant-current STM images (−2 V, 0.1 nA) (a) before and (b) after dissociation of an individual cyclopentene molecule (blue arrow) into two reaction products (green and red arrow). Plots of (c) tunneling current and (d) change in tip height during FCC show an instantaneous drop in current upon dissociation, followed by motion of the tip toward the surface.

densities of these orbitals were summed and a constant-density isosurface was fit to the resulting grid of densities.

Results

Cyclopentene reacts with the Si(100) surface via a [2 + 2]-type reaction,[44,45] resulting in a fully saturated molecule bound to the silicon surface by two covalent Si−C bonds. In a constant-current STM topography image, the cyclopentene molecules appear as protrusions centered on the silicon dimer rows. The FCC technique was applied to an isolated cyclopentene molecule in Figure 1, which shows constant-current (−2.0 V, 0.1 nA) STM topographic images (a) before and (b) after clean desorption (+3.5 V, 3.0 nA) of a cyclopentene molecule from the Si(100) surface. The desorption event can clearly be observed in the tunneling current and tip-height plots in parts (c) and (d), respectively. Upon desorption, the tunneling current immediately decreases from 3.0 to 1.5 nA, followed by the primary feedback loop moving the tip closer to the surface by 0.5 Å in order to reestablish the set point current. The second feedback loop terminates the measurement after the tip movement of 0.5 Å exceeds the ΔZ threshold of 0.2 Å for longer than the specified time ($\Delta t = 0.1$ s).

In addition to clean desorption, cyclopentene dissociation can be captured with FCC as shown in Figure 2. In this case, the stimulation (+3.5 V, 3.0 nA) of the cyclopentene molecule (blue arrow) in Figure 2a by the STM tip yields two reaction products that remain attached to the silicon surface, shown in Figure 2b. One of the adsorbates appears as a protrusion (green arrow), and the other appears as a depression (red arrow) in the STM image (−2.0 V, 0.1 nA). Additionally, the bright feature is no longer centered on the dimer row. The electronic signature of this process can be seen in Figure 2c, where an abrupt drop in the tunneling current from 3.0 to 0.3 nA is detected due to the dissociation of the cyclopentene and the subsequent reduction in the density of states beneath the STM tip. As shown in Figure 2d, the primary feedback loop then responds by advancing the tip ~1.5 Å toward the surface to reestablish the set point current of 3.0 nA. As in Figure 1, the measurement was halted by the second feedback loop after the threshold conditions ($\Delta Z = 0.2$ Å, $\Delta t = 0.1$ s) were exceeded. In this case, the two reaction products of the dissociation process are in immediate proximity to each other.

A second example of cyclopentene dissociation is captured in Figure 3, which also shows a cyclopentene molecule dissociating into two reaction products following an FCC event (+3.5 V, 1.0 nA; $\Delta I = 35\%$, $\Delta t = 100$ μs). However, in this case, the two adsorbates are spatially separated, allowing them to be clearly identified as two distinct surface features for subsequent study. One of the reaction products (green arrow) appears as a protrusion with a similar height to the original cyclopentene molecule (blue arrow), but with a more circular shape and spatially offset from the center of the dimer row. The second reaction product (red arrow) appears as a crescent-shaped depression on one side of the dimer row.

This area of the surface is ideal for further experimental investigation due to the spatial separation of the reaction products as well as the presence of neighboring unperturbed cyclopentene molecules. Consequently, this portion of the surface was imaged with the STM as a function of sample bias from −1.5 to −4.0 V as illustrated in Figure 4. The scan in (a) was taken at −1.5 V and 0.2 nA, and all of the adsorbates exhibit reduced contrast with the background silicon. When the voltage was changed to −2.0 V in (b), the molecules appear similar in appearance to Figure 3b, which was taken at the same

(44) Hamers, R. J.; Hovis, J. S.; Lee, S.; Liu, H. B.; Shan, J. *J. Phys. Chem. B* **1997**, *101*, 1489–1492.
(45) Cho, J. H.; Kleinman, L. *Phys. Rev. B* **2001**, *64*, 235420.

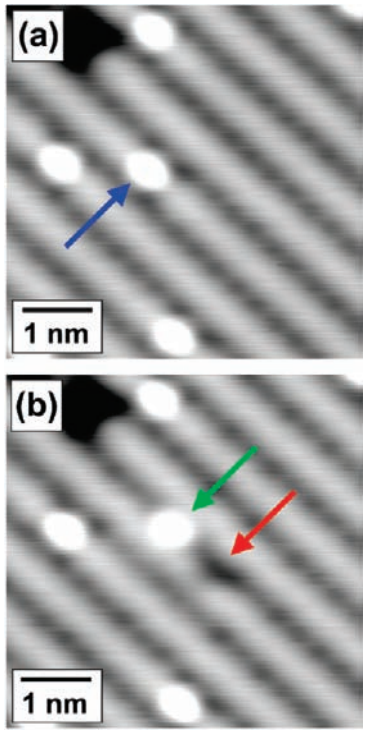

Figure 3. Constant-current STM images (−2 V, 0.2 nA) (a) before and (b) after dissociation (+3.5 V, 1.0 nA) of an individual cyclopentene molecule (blue arrow) into two reaction products: an apparent protrusion (green arrow) and an apparent depression (red arrow). Unperturbed cyclopentene molecules are also present in the image for comparison.

experimental conditions. The voltage was subsequently increased to (c) −2.5 V, (d) −3.0 V, (e) −3.5 V, and (f) −4.0 V, while the tunneling current was held constant at 0.2 nA. The cyclopentene molecules (blue arrows) exhibit increased contrast with the background silicon, and also appear to become more circular at more negative sample biases. The protruding adsorbate (green arrow) also shows increased contrast with the Si(100) surface. It is useful to compare the differences in apparent size and height between the cyclopentene and the protruding reaction product, since this information can be useful in determining differences in the electronic structure of the two adsorbates. In (a), the protruding reaction product (green arrow) appears slightly smaller than the neighboring unperturbed cyclopentene molecule (blue arrow). However, as the magnitude of the voltage is increased, the protruding reaction product appears substantially larger and taller than the cyclopentene molecule. The depressed reaction product (red arrow), on the other hand, does not significantly change in appearance over this range of biases. However, between (d) and (e), the apparent depression switches to the opposite side of the dimer row, where it remains through (f).

In an effort to confirm and better characterize the apparent switching behavior of the depressed reaction product, it was directly probed using the FCC technique as shown in Figure 5. Panel a is an STM image (−2.0 V, 0.2 nA) that shows the adsorbates in the same configuration as in Figure 4f. After this scan, the FCC technique was utilized to trigger the switching event and then subsequently terminate the flow of electrons to prevent additional switching events and/or desorption. In particular, the STM tip was moved directly above the depressed dissociation product (red arrow), and the tunneling conditions were adjusted to −3 V, 1.0 nA with threshold conditions of $\Delta Z = 0.1$ Å and $\Delta t = 1.0$ ms. As expected, an abrupt increase

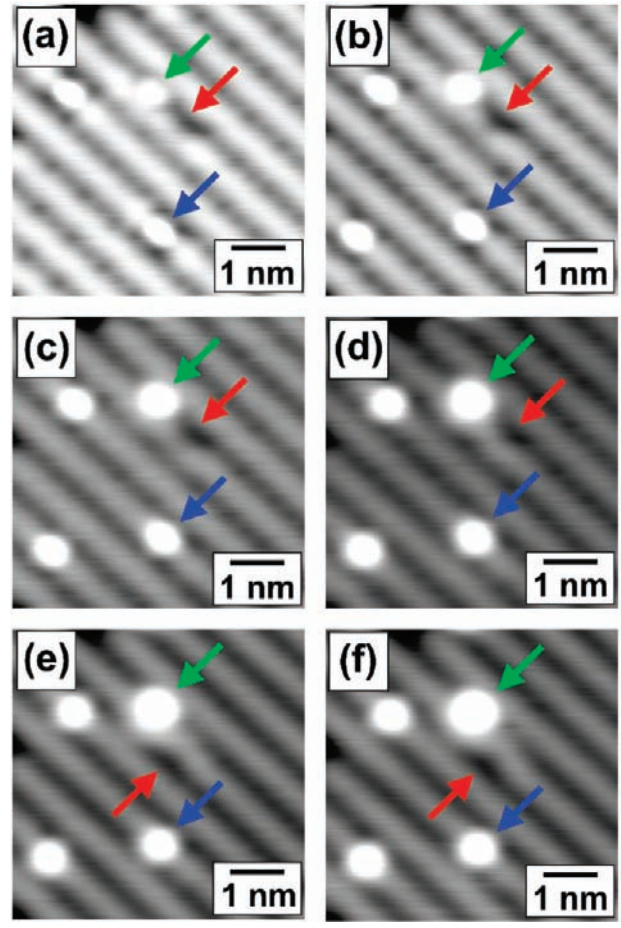

Figure 4. Bias-dependent STM images of cyclopentene dissociation products as well as unperturbed cyclopentene molecules. The images were taken with a tunneling current of 0.2 nA and sample biases of (a) −1.5 V, (b) −2.0 V, (c) −2.5 V, (d) −3.0 V, (e) −3.5 V, and (f) −4.0 V. The depressed reaction product (red arrow) appears qualitatively the same at the different bias conditions, although it switches to the opposite side of the dimer between (d) and (e). Conversely, the apparent size of the protruding dissociation product (green arrow) increases significantly relative to the neighboring unperturbed cyclopentene molecules (blue arrow).

in the tunneling current was detected as the dark feature moved out from underneath the tip, and the flow of tunneling electrons was then terminated by the second feedback loop. Following this event, the same area of the surface was scanned again with the STM at nonperturbative conditions (−2.0 V, 0.2 nA). The resulting image is shown in Figure 5b, which reveals that the depressed dissociation product (red arrow) has indeed returned to its original binding site on the opposite side of the dimer row. It should be noted that this adsorbate can also be induced to completely desorb from the surface by repeating the FCC procedure using a sample bias of +3.5 V and a tunneling current of 3.0 nA.

Discussion

To begin the discussion, it is useful to identify the various features that are present in the STM images. The first feature is the protruding oval-shaped adsorbate (blue arrow), which is centered on the dimer row and can be seen in each STM image. These features are absent during the initial characterization of the clean Si(100) surface, and appear only after dosing the surface with cyclopentene in the UHV chamber. Consequently, these adsorbates are identified as cyclopentene molecules that

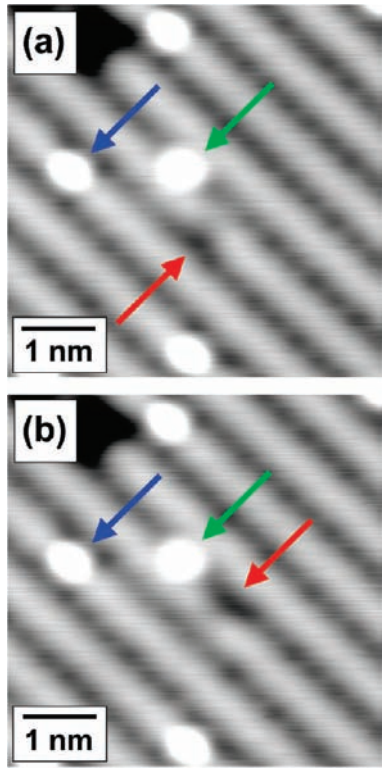

Figure 5. Constant-current STM images (−2 V, 0.2 nA) of unperturbed cyclopentene molecules (blue arrow) and cyclopentene dissociation products (green arrow and red arrow). The same area of the surface is shown (a) before and (b) after STM-induced hopping of the depressed reaction product (red arrow) to the opposite atom of the silicon dimer.

have chemisorbed to the Si(100) surface. The process observed in Figures 2 and 3 is consistent with an STM-induced dissociation reaction of cyclopentene on Si(100). The dissociation reaction yields two products, which appear as a protrusion (green arrow) and depression (red arrow). The depressed dissociation product possesses properties consistent with an isolated hydrogen atom on the Si(100) surface. In particular, hydrogen is known to have a reduced density of states compared to a clean silicon dangling bond, thus leading to its appearance as a depression on the Si(100) surface.[17] Second, the STM-induced movement of the depressed reaction product in Figures 4 and 5 can be explained by the hopping of a hydrogen atom between the two different silicon atoms of the same dimer. This STM-triggered switching behavior for an isolated hydrogen atom on a silicon dimer has been previously reported under similar imaging conditions.[46] Finally, the depressed dissociation product is observed to desorb at +3.5 V, 3.0 nA, which is consistent with previous reports of electron-stimulated desorption of hydrogen from passivated Si(100).[17] Consequently, it is concluded that this reaction product is an isolated hydrogen atom chemisorbed to the Si(100) surface.

On the other hand, the second dissociation product (green arrow) appears as a protrusion that is offset from the center of the dimer row as seen in Figures 2−5. Assuming that the depressed reaction product is a single hydrogen atom chemisorbed to the Si(100) surface, then the protruding dissociation product is expected to be the remaining C_5H_7 fragment that is tethered to the surface via a single Si−C bond. Several

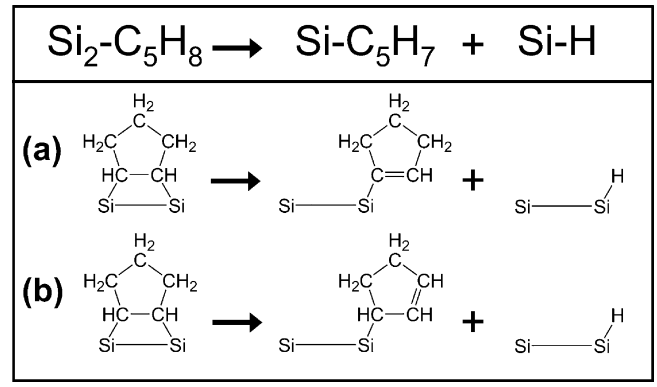

Figure 6. Potential dissociation reactions for $C_5H_8 \rightarrow C_5H_7 + H$, showing two stable C_5H_7 fragments. In both cases, a C=C double bond forms, and the C_5H_7 fragment remains bound to the silicon surface via a single Si−C bond.

configurations of Si−C_5H_7 are possible, depending on which hydrogen dissociates from the original cyclopentene molecule. Dissociation reactions from each of the five carbon atoms of the cyclopentene ring were initially considered, and DFT calculations were employed to determine whether or not the proposed reaction products represent minima on the potential energy surface. The two most energetically favorable configurations are shown in Figures 6a and b, in which the products of the dissociation reaction result in a cyclopentene analog with an intact C=C double bond. Two other possible reactions result in diradical reaction products, which were found to be significantly higher in energy than those with a C=C bond and thus were not further considered. The fifth possibility for the dissociation reaction yields a lone pair on one of the carbon atoms. However, this configuration was found to be unstable within DFT and was therefore ruled out. Additional evidence for the identity of the Si−C_5H_7 can be obtained from the bias-dependent imaging data in Figure 4. In particular, the distinct increase in the apparent size and height of the C_5H_7 fragment as a function of sample bias indicates a sharp increase in the local density of states, which is much more rapid and pronounced than in the di-σ bonded cyclopentene molecule. This observation illustrates the difference in the orbital structure of the two adsorbates, and is consistent with the presence of a low-lying π orbital in the C_5H_7 molecule.

The reaction from Figure 6a is explored further in Figure 7, which shows the DFT-optimized geometries of the isolated reactant and products of the cyclopentene dissociation reaction on a $Si_{21}H_{20}$ cluster. Figure 7a shows the global minimum configuration of cyclopentene on Si(100), which is in good agreement with previous reports of cyclopentene on silicon.[47] The lowest energy configuration of the C_5H_7 fragment bound to the silicon surface via a single Si−C bond (Figure 6a) is shown in Figure 7b. The presence of the C=C double bond can be inferred from the coordination number of the carbon atoms and from the bond lengths and angles. Finally, the dissociated hydrogen atom bonded to a single silicon dimer atom is shown in Figure 7c.

To directly compare these structures with the experimental STM data, simulated STM images were calculated within DFT using the Tersoff-Haman approximation[48] as shown in Figure

(46) Quaade, U. J.; Stokbro, K.; Thirstrup, C.; Grey, F. *Surf. Sci.* **1998**, *415*, L1037−L1045.
(47) Cantele, G.; Trani, F.; Ninno, D.; Cossi, M.; Barone, V. *J. Phys.: Condens. Matter* **2006**, *18*, 2349–2365.
(48) Tersoff, J.; Hamann, D. R. *Phys. Rev. Lett.* **1983**, *50*, 1998–2001.

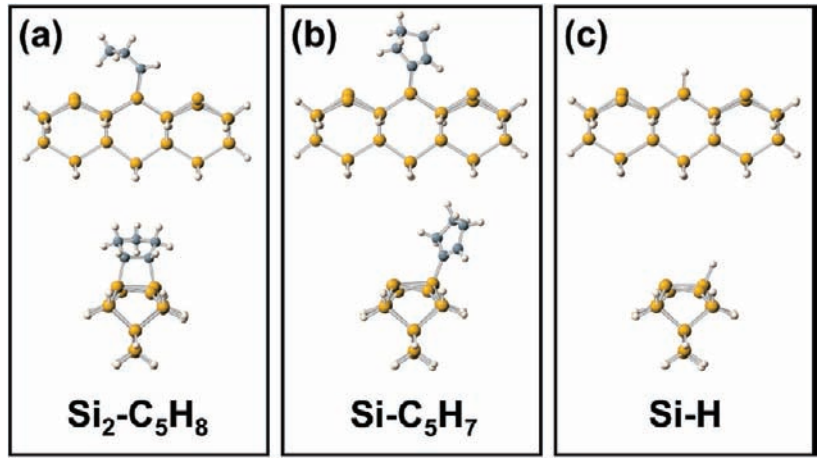

Figure 7. Optimized DFT geometries of the reactants and products of the cyclopentene dissociation reaction on a three-dimer $Si_{21}H_{20}$ cluster. (a) Individual cyclopentene molecule bound to the Si(100) surface via two covalent Si−C bonds prior to dissociation. The lowest-energy C_5H_7 isomer from Figure 6 is shown in b, bound via a single Si−C bond. (c) Second dissociation product (a single H atom) bound to the Si(100) surface.

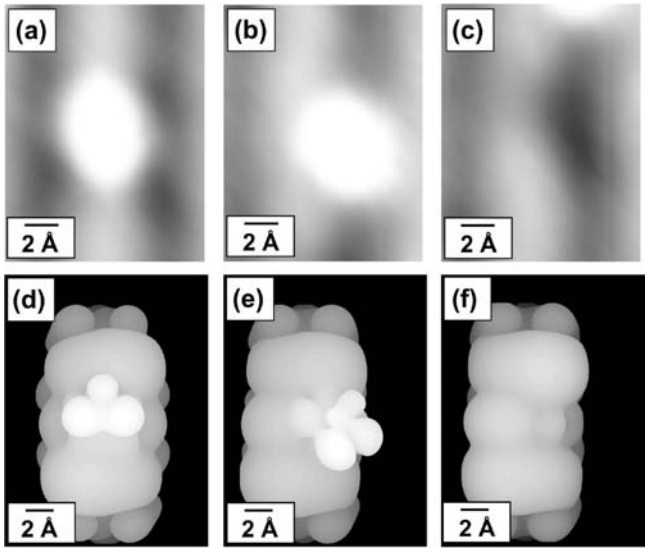

Figure 8. Experimental (a−c) and calculated (d−f) STM images of the cyclopentene dissociation reactants and products. The experimental constant-current images were taken at −2 V, 0.1 nA and show (a) the di-σ bonded cyclopentene molecule (appears as a protrusion centered on the silicon dimer row), (b) the C_5H_7 product (appears as a protrusion offset from the center of the silicon dimer row), and (c) the H atom product (appears as a depression offset from the center of the silicon dimer row). Similarly, the bottom row consists of simulated STM images of (d) cyclopentene, (e) C_5H_7, and (f) H atom. The simulated STM images were generated from the equilibrium geometries shown in Figure 7 using an isosurface value of 1×10^{-5} e/a_o^3.

8. Panels a, b, and c represent a zoom-in view of the STM topographic data from Figure 3b, showing (a) the cyclopentene molecule in the standard di-σ bonded configuration, (b) the C_5H_7 fragment, and (c) the isolated hydrogen atom. Panels d−f represent the simulated STM images, showing (d) the global minimum di-σ structure (Figure 7a), (e) the singly bonded C_5H_7 fragment (Figure 7b), and (f) an isolated hydrogen atom (Figure 7c) on the clean Si(100) surface. All of the images were generated using an isosurface value of 1×10^{-5} e/a_o^3. Direct comparison of the two sets of data shows that the simulated images are in good agreement with the experimental STM data. One subtle difference is observable in the di-σ bonded case (Figure 8a and d), where the bright protrusion associated with the cyclopentene molecule in the simulated image appears more localized and asymmetric than its counterpart in the experimental image. One explanation for this discrepancy is that tunneling electrons from the STM tip can induce a rotational or vibrational motion of the molecule about the Si−Si dimer bond, causing the molecule to have a more elliptical shape along the dimer row in the STM image than in the corresponding simulated image. It should be noted that this elliptical shape for isolated cyclopentene molecules on Si(100) has been observed in previous STM studies.[49] In the case of the C_5H_7 fragment, the agreement between the calculation and the experiment is even closer, with the fragment appearing as a bright protrusion off-center from the silicon dimer row in both cases. Small differences exist between Figure 8b and e, such as the C_5H_7 appearing larger and rounder in the experimental image than the calculation. This subtle discrepancy can be attributed to tip convolution effects or the possibility of rotational motion about the single Si−C bond tethering the C_5H_7 to the surface. Finally, the experimental and calculated images of the single hydrogen atom on Si(100) are also in good agreement, with the hydrogen appearing as a crescent-shaped depression in both cases. Furthermore, the results shown in Figure 8c and f are consistent with previous experimental reports of hydrogen on clean Si(100).[50,51] Overall, the strong agreement between the experimental and simulated STM images supports the cyclopentene dissociation reaction proposed in Figure 6.

Conclusions

In summary, this paper has examined the STM-triggered dissociation reaction of cyclopentene on the Si(100) surface. The FCC approach allowed the STM electron dose to be precisely regulated, thus avoiding overdosing of the reaction products. In this manner, the dissociation products could be isolated and subjected to further interrogation including multibias STM imaging and additional FCC. For example, FCC was used to reversibly manipulate single hydrogen atoms between two atomic surface sites and to irreversibly desorb hydrogen from the surface. Additionally, DFT calculations were performed to

(49) Hamers, R. J.; Hovis, J. S.; Greenlief, C. M.; Padowitz, D. F. *Jpn. J. Appl. Phys. Part 1* **1999**, *38*, 3879–3887.
(50) Vasek, J. E.; Zhang, Z. Y.; Salling, C. T.; Lagally, M. G. *Phys. Rev. B* **1995**, *51*, 17207–17210.
(51) Hu, Z. H.; Biedermann, A.; Knoesel, E.; Heinz, T. F. *Phys. Rev. B* **2003**, *68*, 155418.

compare various possible reaction products and to generate simulated STM images, ultimately allowing identification of the cyclopentene dissociation products as C_5H_7 and H. Overall, this case study of cyclopentene dissociation on Si(100) highlights the utility of the FCC technique for the study of single molecule chemistry with the STM, thus suggesting its use for other adsorbates on semiconductor surfaces. In this manner, FCC is expected to elucidate a variety of fundamental surface chemical reactions that are central to the fields of molecular electronics, chemical and biological sensing, molecular actuation, and catalysis.

Acknowledgment. This work was supported by the National Science Foundation (Award Numbers EEC-0647560, DMR-0520513, and ECS-0506802) and the Office of Naval Research (Award Numbers N00014-05-1-0563 and N00014-09-1-0180). We thank Tamar Seideman and Liam Palmer for helpful discussions and Joseph Lyding for the use of his STM control software.

Supporting Information Available: Complete author list for ref 42. This material is available free of charge via the Internet at http://pubs.acs.org.

JA9010546